The 9th European Congress on Computational Methods in Applied Sciences and Engineering
ECCOMAS Congress 2024
3–7 June 2024, Lisboa, Portugal

CHARACTERIZING NUMERICAL SURFACE TENSION IN THE CONSERVATIVE VOLUME-OF-FLUID METHOD

Tzu-Yao Huang[1*], Artur K. Lidtke[2], Kelli L. Hendrickson[3], Thomas J. C. van Terwisga[1,2], and Gabriel D. Weymouth[1]

[1] Faculty of Mechanical Engineering, Delft University of Technology, Mekelweg 2, 2628CD Delft, the Netherlands, {T.-.Y.Huang, G.D.Weymouth}@tudelft.nl

[2] Maritime Research Institute Netherlands (MARIN), P.O. Box 28, 6700AA Wageningen, the Netherlands, {A.Lidtke, T.v.Terwisga}@marin.nl

[3] Carolina Center for Interdisciplinary Applied Mathematics, University of North Carolina at Chapel Hill, Chapel Hill, NC, USA, drkh@email.unc.edu

Key words: Multiphase Flows, Geometric Volume-of-Fluid Method, Numerical Surface Tension

Summary. In simulations of weak-surface-tension multiphase flows, the fine-scale of multiphase structures can be under-resolved due to finite size of the numerical grid. These limits can induce quasi-surface-tension effects, known as numerical surface tension, which are particularly pronounced in geometric Volume-of-Fluid (gVoF) methods [1, 2]. This study systematically characterizes this effect with a specific focus on the conservative Volume-of-Fluid (cVoF) approach [3]. Several pure passive advection cases are investigated to identify the mechanism, while also exploring the influence of different interface normal reconstruction schemes.

The discontinuities in the reconstructed interface between adjacent grid cell faces are found to drive numerical surface tension, as demonstrated by a series of pure advection test-cases. Errors in the surface normal direction reconstruction scheme are shown to exacerbate this effect, as shown in the simple case of reconstructing a circular droplet.

Like physical surface tension, the numerical surface tension effect scales linearly with grid-based curvature. The time scale of the numerical surface tension effect is governed by a diffusion mechanism rather than wave propagation as in the case of physical surface tension. Nevertheless, the final effect on the flow is similar for both. The kinematics of interface structures smaller than $\mathcal{O}(10)$ grid lengths is found to be most influenced by the numerical surface tension.

1 INTRODUCTION

Multiphase flows ubiquitously occur in marine environments, such as air entrainment in breaking waves [4], and in everyday engineering applications like ink-spray technology [5]. To understand the phenomena, numerical simulations are widely applied to analyze interface dynamics and statistics.

Among several multiphase numerical schemes, geometric Volume of Fluid (gVoF) method is particularly often chosen for its capability to preserve the interface sharpness below the grid size. This method reconstructs surfaces in each interfacial cell for advecting the volume fraction. The sub-grid interface shape can vary in complexity from low to high order: a vertical/horizontal

plane (Simple Line Interface Calculation, SLIC) [6], a plane (Piecewise Linear Interface Calculation, PLIC) [7], a dog-eared plane (Bilinear Interface Calculation, BLIC) [8], or a paraboloid (Piecewise Parabolic Interface Calculation, PPIC) [9]. To balance computational cost and accuracy, PLIC is typically chosen. Furthermore, to conserve the mass, this study incorporates conservative Volume-of-Fluid (cVoF) [3] approach, an operator-splitting PLIC-gVoF.

Applying PLIC-gVoF sometimes results in numerical surface tension. Rudman [10] observed shape changes when purely advecting droplets with different normal estimation schemes. Research on thin film dynamics has also revealed another aspect of numerical surface tension: failure to resolve the dynamics of multiphase structures smaller than grid size [1, 2]. For example, when the liquid film thickness is thinner than the grid size, none of the existing interface reconstruction schemes can accurately capture the interface, leading to artificial rupture of the thin film. These numerical artifacts resemble those arising due to the action of physical surface tension. Thus, the effect is called numerical surface tension.

The behavior of PLIC is significantly influenced by the estimation of the normal vector, as the interface topology is fully determined by the plane direction and volume fraction. Several schemes have been presented in the literature [3, 7, 11, 12, 13], the differences between which will be investigated in this study.

This research focuses on shape change effect due to pure advection, similarly to the work of [10]. This is done to allow fundamental observations to be made about the numerical surface tension effects in the absence of other factors typically affecting complete fluid flow simulations. In particular, this study investigate several attributes of the numerical surface tension – mechanism, effects, time and length scales.

2 CONSERVATIVE VOLUME-OF-FLUID METHOD

Only the multiphase advection equation is utilised in the present study as the multiphase structures are purely advected [10]. VoF method uses a color function, $c(\mathbf{x})$, to indicate different fluid regions: 1 for "dark" fluid while 0 for "light" fluid. Assuming the two fluids are immiscible, the color function follows the material transportation law to be written:

$$\frac{\mathrm{D}c}{\mathrm{D}t} = \frac{\partial c}{\partial t} + \mathbf{u} \cdot \nabla c = 0, \tag{1}$$

where $\mathbf{u}$ is the flow velocity vector. The gradient of c is not defined at the interface, but integrating the differential equation over a cell eases this issue:

$$\frac{\partial}{\partial t} \int_\Omega c \, \mathrm{d}V + \oint_{\partial\Omega} c \, \mathbf{u} \cdot \hat{\mathbf{n}} \, \mathrm{d}S = \int_\Omega c \, \nabla \cdot \mathbf{u} \, \mathrm{d}V. \tag{2}$$

In discrete calculations, the water volume fraction (f) of a computational cell Ω is defined as

$$f = \frac{\int_\Omega c \, \mathrm{d}V}{\int_\Omega \mathrm{d}V}. \tag{3}$$

Thus, the integral form becomes:

$$\Delta\Omega \frac{\partial f}{\partial t} + \mathfrak{F} = \int_\Omega c \, \nabla \cdot \mathbf{u} \, \mathrm{d}V, \tag{4}$$

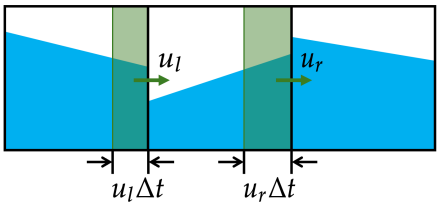

Figure 1: Example of geometric advection for a 1D case. Dark fluid occupies the blue area. The shaded green rectangles, also known as advection sweep, are fluid going to be advected to the next cell after a time step of Δt. u_l and u_r denote the velocities upon the corresponding faces.

where $\Delta\Omega$ is the cell volume and $\mathfrak{F}$ is the net water volume flux from all faces.

However, to avoid repeated advection, the transport equation is split by direction and sequentially integrated to the next time step:

$$\begin{aligned}
\Delta\Omega\left(f^{(*)}-f^{(n)}\right) &= \Delta t\left(\mathfrak{F}_x + c_c\frac{\partial u}{\partial x}\Delta\Omega\right);\\
\Delta\Omega\left(f^{(**)}-f^{(*)}\right) &= \Delta t\left(\mathfrak{F}_y + c_c\frac{\partial v}{\partial y}\Delta\Omega\right);\\
\Delta\Omega\left(f^{(n+1)}-f^{(**)}\right) &= \Delta t\left(\mathfrak{F}_z + c_c\frac{\partial w}{\partial z}\Delta\Omega\right).
\end{aligned} \tag{5}$$

Here, $\mathfrak{F}_d$ is the flux on the corresponding faces of direction d, and coefficient of dilation term reads:

$$c_c = \begin{cases} 1 & \text{if } f^{(n)} > 0.5;\\ 0 & \text{if } f^{(n)} \leq 0.5. \end{cases} \tag{6}$$

The dilation term is preserved to account for and redistribute extra flux across directions.

During each directional advection step, piecewise-linear interfaces are reconstructed, and an upwind donor-acceptor scheme determines the advected part, as shown in Fig. 1. The dark fluid (blue part), covered by the advection volume (green shade), will be advected from the donor cell to the acceptor cell. The advection volume is a rectangular sweep with a width of velocity times the time step.

In the reconstruction step, the interface normal vectors are estimated to describe the interface shape. This study focuses on four estimation schemes: Pure Central Difference (PCD), Column Difference (CD), Weymouth-Yue (WY, [3]), and Mixed Youngs-Centered (MYC, [11]). PCD and CD use finite difference calculations as shown in Fig. 2, while WY and MYC are height-function-based calculations with several selection criteria.

3 ADVECTION TEST CASE

Rudman [10] advected several shapes in 2D with unidirectional velocity fields on a uniform square grid. His study found that when the velocity field deviated from the mesh directions, by approximately 26.5° in his case, it caused the most severe shape distortion.

To facilitate more fundamental observations and develop simple models, a simpler test case called “Pac-Man” is investigated here, where a solid circular multiphase structure is advected

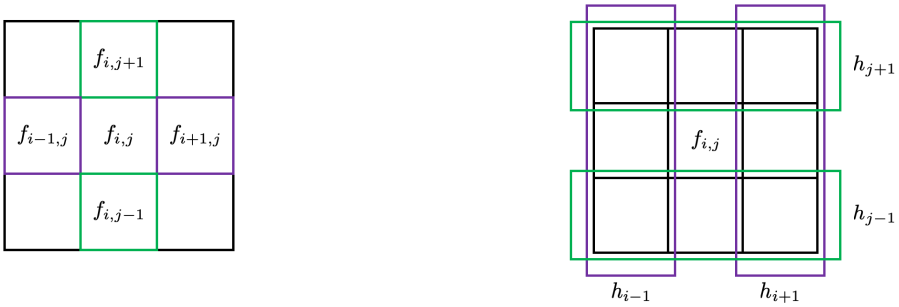

(a) Pure central difference.

(b) Column difference.

Figure 2: Estimation of normal vector value. The magnitude of x and y normal vector components are determined by the central difference between volume fraction inside purple and green areas, respectively.

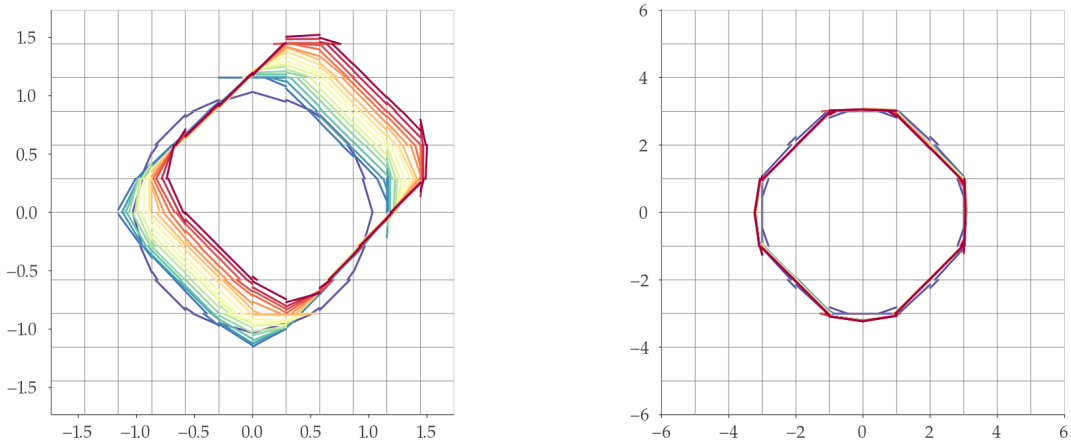

(a) Pac-Man.

(b) Shaking.

Figure 3: Overlapped reconstructed interfaces whenever the droplet finishes one domain cycle in Pac-Man test case or returns to original position for shaking test case. Time evolves from blue to yellow to red. The normal estimation scheme here is PCD.

along the diagonal direction (45°) inside a periodic domain. It is noteworthy that, again, only the volume fraction advection equation is used, with no dynamics nor physical surface tension included.

However, tracking intricate shape changes in the Pac-Man test is challenging as the shape is not fixed to one location. Therefore, a new test case, called "shaking," is introduced, where the velocity direction alternates between 45° and 225° at each time step. This test case brings the droplet back to its original position every other time step, rather than seeing it continuously move as in the Pac-Man case.

Fig. 3 verifies that shaking test case behave similarly to Pac-Man one regarding shape changes. Both converge to a similar shape, apart from the shape drift in the Pac-Man test due to a constant bias in one direction. These two test cases are also conceptually equivalent to a sufficient extent. Whenever a shape is advected by the length of a grid cell in the Pac-Man test, it can be artificially shifted back by one grid cell without altering any interface topology. Advecting a cell and shifting it back essentially constitutes shaking with an amplitude of half a grid size, justifying the shaking test case.

The following sections will thus be based on the results of the shaking test cases. Unless explicitly stated otherwise, the Courant–Friedrichs–Lewy (CFL) number is chosen as:

$$\mathrm{CFL} = \frac{|u|\Delta t}{\Delta x} = \frac{|v|\Delta t}{\Delta x} = \frac{1}{12}, \tag{7}$$

where u and v are velocities in x, y direction, while Δx and Δt represent the spatial and temporal discretization sizes.

4 CLUES OF NUMERICAL SURFACE TENSION

Two noticeable phenomena emerge from the test cases, as depicted in Fig. 4:

1. Droplet converges to a distinct shape, depending on the chosen normal estimation scheme.
2. Discontinuities of the reconstructed interfaces at cell faces tend to diminish or resolve.

These observations qualitatively resemble physical surface tension, which smooths out discontinuities and makes continuous fluid structures adopt particular shapes, such as a circle for the common case of uniform surface tension.

The first observation, where a shape is influenced by the normal estimation scheme, could be explained through a static reconstruction test case. A quarter circle is reconstructed via several different normal estimation schemes, and comparing their sub-grid interface orientations with theoretical values yiedls Fig. 5. This comparison determines the converged shape seen in Fig. 4. For instance, the PCD scheme biases normal estimation towards 45°, resulting in a final shape characterized by inclined straight lines. This underscores the importance of selecting appropriate normal estimation schemes to mimic uniform-surface-tension flow.

The second observation, concerning diminishing discontinuities, relates to the mechanism driving numerical surface tension. As discontinuities shrink, akin to a rubber band, there is an opportunity to reshape the multiphase structure until it matches the stable shape determined by the normal reconstruction scheme mentioned earlier. Further investigation into background mechanisms and conceptual models will be conducted to analyze time and length scales in the subsequent section.

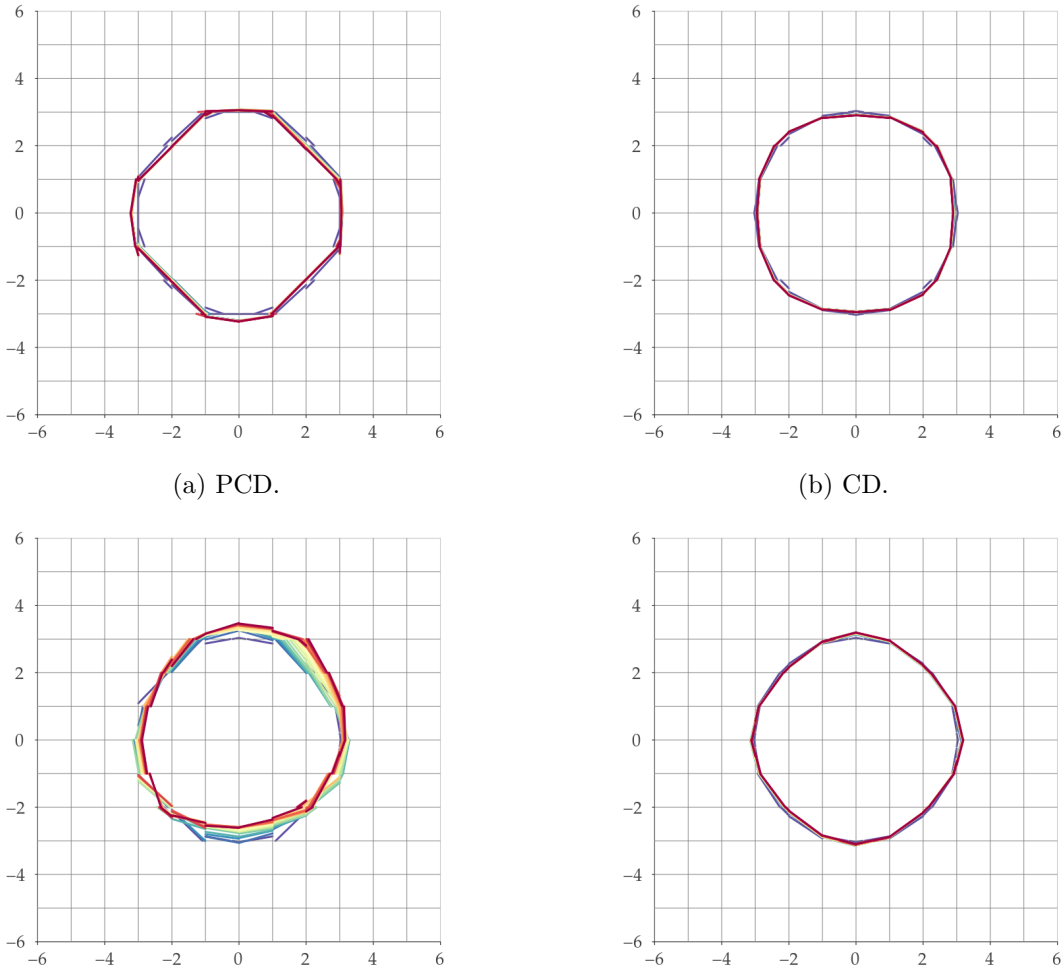

(a) PCD.

(b) CD.

(c) WY.

(d) MYC.

Figure 4: Overlapped shapes of different normal estimation schemes across simulation time. Total normalized absolute advection distance is $|\mathbf{u}|t/\Delta x = 30\sqrt{2}$. PCD: pure central difference; CD: column difference; WY: Weymouth-Yue; MYC: mixed Youngs-Centered.

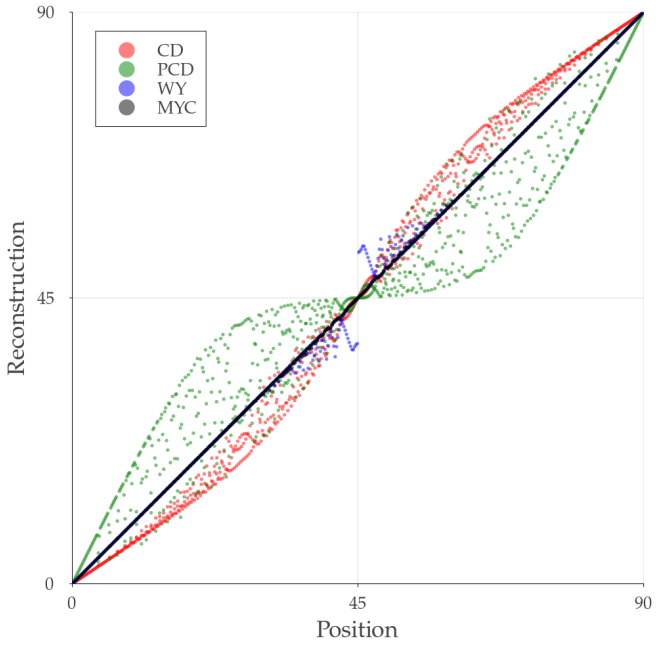

Figure 5: Comparison of normal estimation schemes reconstructing a circular droplet. Ideal behavior is denotes as the diagonal line: Position = Reconstruction.

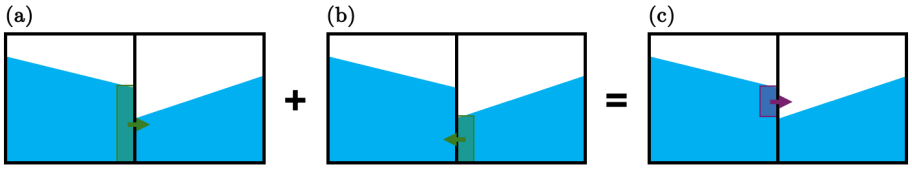

Figure 6: Demonstrates how discontinuities disappear under the shaking test case. (a) and (b) shows two consecutive time steps, while (c) demonstrates the net effect from those two time steps together.

5 BACKGROUND MECHANISM & TIME AND LENGTH SCALE ANALYSIS

The previously observed discontinuities drive the numerical surface tension. A simple one-dimensional shaking thought experiment (Fig. 6) illustrates that these discontinuities tend to smooth themselves out. After two consecutive time steps in the shaking case, a net flux is generated from higher to lower water levels, proportionally to the length of the discontinuity. This quantifies the strength and length scale of numerical surface tension, where the driving effect is directly proportional to the discontinuity length.

Further characterization of the relationship between discontinuity and length scale could be illustrated by static reconstruction of a circular droplet in different resolutions (Fig. 7). This analysis shows that the discontinuity length per unit circumference increases linearly with grid-based curvature, aligning with physical surface tension length scales.

For time scale analysis, a pure horizontal interface reconstruction is further assumed in a

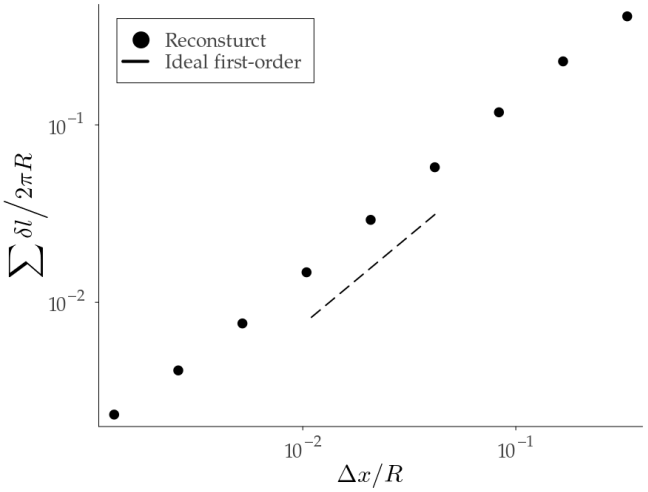

Figure 7: Discontinuity length per circumference length versus grid-based radius under the reconstruction of MYC. The dots denote discontinuity length and the dashed line represents linear dependency, power of one.

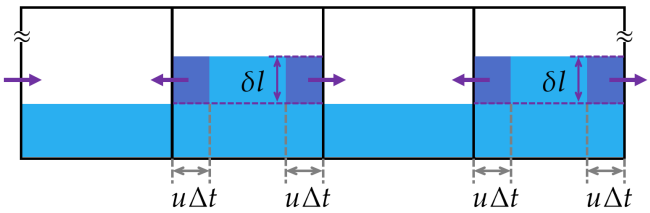

Figure 8: Net flux (purple shaded area) between neighborhood cells with discontinuity δl after two consecutive time steps, $2\Delta t$. The periodic boundaries at both sides are imposed.

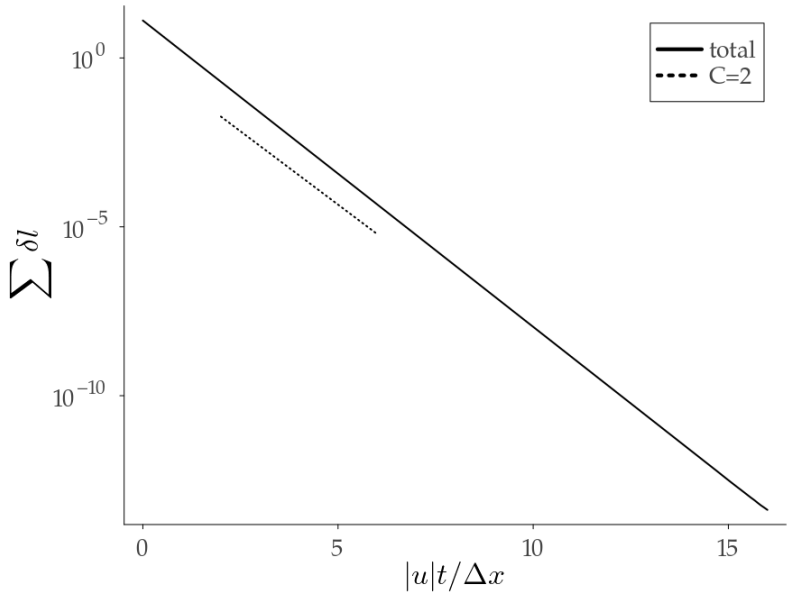

Figure 9: Temporal convergence plot of discontinuity length of Fig. 8. The ideal slope of $C = 2$ is indicated as the dashed line.

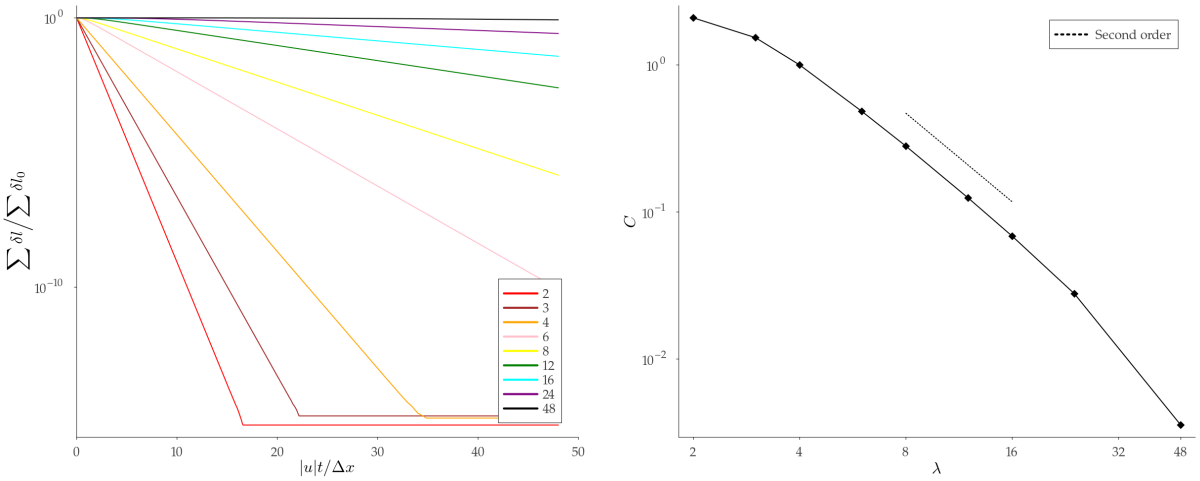

Figure 10: Quantifying length scale and time scale of different wavelength (λ). The left panel shows the convergence of the total discontinuity length with different wavelength, signified by different colors. The right panel extracts C in the form of $\delta l \sim \exp(-C|u|t/\Delta x)$ from different wavelength and plots them in log-log plot. The dashed line is $C \sim \lambda^{-2}$.

one-dimensional shaking thought experiment. This setup includes periodic boundary conditions with a wave of wavelength $2\Delta x$ (Fig. 8). Assuming mild interface changes across time steps, the evolution of each discontinuity after two consecutive time steps follows:

$$\delta l^{(i+2)} = \delta l^{(i)} - 4\delta l^{(i)} \frac{|u|\Delta t}{\Delta x}. \tag{8}$$

This evolution resembles a differential equation:

$$\frac{\mathrm{d}\delta l}{\mathrm{d}t} = -2\frac{|u|}{\Delta x}\delta l, \tag{9}$$

with the solution:

$$\delta l \sim e^{-2|u|t/\Delta x}. \tag{10}$$

The exponential nature of the derived model and coefficient 2 in exponent is confirmed by the numerical simulation (Fig. 9).

In order to generalize the result to different length scale, wave length (λ) here, three consecutive grid cells ($i-1$, i, $i+1$) are examined in detail. The volume fraction of the central cell (f_i) after the first time step with positive velocity is:

$$\frac{f_i^{(n+1)} - f_i^{(n)}}{\Delta t} = -|u|\frac{f_i^{(n)} - f_{i-1}^{(n)}}{\Delta x}. \tag{11}$$

After the second time step with negative velocity:

$$\frac{f_i^{(n+2)} - f_i^{(n+1)}}{\Delta t} = +|u|\frac{f_{i+1}^{(n+1)} - f_i^{(n+1)}}{\Delta x}. \tag{12}$$

Assuming mild changes in volume fraction across time steps, the two equations sum yields:

$$\frac{f_i^{(n+2)} - f_i^{(n)}}{2\Delta t} \approx \frac{|u|\Delta x}{2}\frac{f_{i+1} - 2f_i + f_{i-1}}{\Delta x^2} \quad \Longrightarrow \quad \frac{\partial f}{\partial t} = \frac{|u|\Delta x}{2}\frac{\partial^2 f}{\partial x^2}. \tag{13}$$

Thus, the solution resembles

$$f(x,t;k) \sim e^{-0.5(k\Delta x)^2|u|t/\Delta x}\sin(kx), \tag{14}$$

where $k\Delta x$ is the grid-based wavenumber, defined as $2\pi\Delta x/\lambda$.

The discontinuity equation (Eq. 9) can be recovered from Eq. 13. The discontinuity at x_0 is the difference between volume fractions at $x \pm \Delta x/2$:

$$\delta l = \Delta x \cdot f\left(x_0 + \frac{\Delta x}{2}\right) - \Delta x \cdot f\left(x_0 - \frac{\Delta x}{2}\right) \approx \frac{\partial f}{\partial x}\Delta x^2. \tag{15}$$

Taking the partial derivative of Eq. 13 in x and assuming the spatial part of the solution reads $\cos(kx)$ (cf. Eq. 14) yields

$$\frac{\partial \delta l}{\partial t} = \frac{|u|}{2}\frac{\partial^2 \delta l}{\partial x^2} = -\frac{|u|}{2\Delta x}(k\Delta x)^2\delta l. \tag{16}$$

The developed equation is successfully verified in Fig. 10, where the convergence speed of total discontinuity is plotted against the wavelength, matching the speed predicted by $(k\Delta x)^2$.

From the analysis, the relationship between length ($\mathcal{L}$) and time ($\mathcal{T}$) scales are established:

$$\mathcal{T} \sim \frac{\Delta x}{(k\Delta x)^2|u|} \Longrightarrow \frac{|u|\mathcal{T}}{\Delta x} \sim \left(\frac{\mathcal{L}}{\Delta x}\right)^2, \tag{17}$$

which means time scale depends on square of the grid-based length scale ($\mathcal{L}/\Delta x$). However, the time scale associated with physical surface tension, derived from capillary water waves [14], differs:

$$\omega^2 = \frac{\eta}{\rho}k^3 \quad \Longrightarrow \quad \mathcal{T} \sim \mathcal{L}^{1.5}, \tag{18}$$

where η and ρ denote the surface tension coefficient and density, respectively. The time scales deviate as numerical surface tension is a diffusion mechanism without inertial effect. Meanwhile, scales of physical surface tension come from the balance between inertial forces and cohesion effects. Further refinement of the model or inclusion of relevant physics in a more delicate test case is needed to adequately compare the time scales.

6 CONCLUSION AND OUTLOOK

This study reveals that the gVoF method exhibits numerical surface tension due to discontinuities in reconstructed interfaces. This results in a characteristic converged shape after advection determined by the normal estimation scheme. This effect scales linearly with grid-based curvature, akin to physical surface tension. However, its time scale is proportional to the square of the length scale, contrasting with the 1.5 power dependency in physical surface tension.

While the tests are performed with the operator-split PLIC gVoF method, these findings suggest that any similar method, even an unsplit advection scheme, involving interface discontinuities or frequent normal reconstruction, may suffer from numerical surface tension, albeit up to differing time scales. For instance, schemes like PPIC may still exhibit discontinuities, and BLIC suffers from reconstruction biases and therefore will experience numerical surface tension effects but to a milder extent than PLIC.

Numerical surface tension becomes significant when multiphase structures are not resolved well. This effect might happen in simulations with low to negligible physical surface tension. However, accurately quantifying numerical surface tension may allow one to emulate physical surface tension at grid length scales in simulations with high Weber numbers such that similar statistic could be recovered without including physical surface tension. This idea is qualitatively similar to using grid-induced numerical dissipation in implicit LES.

REFERENCES

[1] A. Han and O. Desjardins, "Subgrid-scale modeling of droplet bag breakup." 76th APS DFD [presentation], 2023.

[2] P. Hergibo, T. N. Phillips, and Z. Xie, "A moment-of-fluid method for resolving filamentary structures using a symmetric multi-material approach," *Journal of Computational Physics*, vol. 491, p. 112401, 2023.

[3] G. Weymouth and D. K.-P. Yue, "Conservative volume-of-fluid method for free-surface simulations on cartesian-grids," *Journal of Computational Physics*, vol. 229, no. 8, pp. 2853–2865, 2010.

[4] G. B. Deane and M. D. Stokes, "Scale dependence of bubble creation mechanisms in breaking waves," *Nature*, vol. 418, pp. 839–844, Aug. 2002.

[5] C. Constante-Amores, L. Kahouadji, A. Batchvarov, S. Shin, J. Chergui, D. Juric, and O. Matar, "Direct numerical simulations of transient turbulent jets: vortex-interface interactions," *Journal of Fluid Mechanics*, vol. 922, p. A6, 2021.

[6] C. W. Hirt and B. D. Nichols, "Volume of fluid (vof) method for the dynamics of free boundaries," *Journal of computational physics*, vol. 39, no. 1, pp. 201–225, 1981.

[7] D. L. Youngs, "Time-dependent multi-material flow with large fluid distortion," *Numerical methods for fluid dynamics*, 1982.

[8] M. van der Eijk and P. Wellens, "An efficient bilinear interface reconstruction algorithm and consistent multidimensional unsplit advection scheme for accurate capturing of highly-curved interfacial shapes on structured grids," *Journal of Computational Physics*, vol. 498, p. 112656, 2024.

[9] G. R. Price, *A piecewise parabolic volume tracking method for the numerical simulation of interfacial flows*. University of Calgary Calgary, AB, 2000.

[10] M. Rudman, "Volume-tracking methods for interfacial flow calculations," *International Journal for Numerical Methods in Fluids*, vol. 24, pp. 671–691, Apr. 1997.

[11] E. Aulisa, S. Manservisi, R. Scardovelli, and S. Zaleski, "Interface reconstruction with least-squares fit and split advection in three-dimensional cartesian geometry," *Journal of Computational Physics*, vol. 225, no. 2, pp. 2301–2319, 2007.

[12] E. G. Puckett, "A volume-of-fluid interface tracking algorithm with applications to computing shock wave refraction," in *proceedings of the fourth international symposium on Computational Fluid Dynamics*, pp. 933–938, Mathematical Sciences Publishers Davis, CA, 1991.

[13] J. E. Pilliod, *An analysis of piecewise linear interface reconstruction algorithms for volume-of-fluid methods*. University of California, Davis, 1992.

[14] R. G. Dean and R. A. Dalrymple, *Water wave mechanics for engineers and scientists*. World Scientific, 1991.